Blueprint for wafer-scale three-dimensional photonic band-gap synthesis by photoelectrochemical etching

Timothy Y. M. Chan and Sajeev John
Department of Physics, University of Toronto, 60 St. George Street, Toronto, Ontario, Canada M5S 1A7
(Received 10 February 2003; published 21 October 2003)

We present an architecture for three-dimensional photonic band-gap (PBG) material synthesis by oblique angle photoelectrochemical pore etching. This technique provides high aspect ratio pores, in which the pore diameter can be modulated by changing light intensity during the etch process. The naturally occurring ''Kielovite'' structure is a stretched version of the face-centered-cubic lattice of crisscrossing pores and exhibits a PBG to center frequency ratio of 8% in a background dielectric constant of 11.9 (silicon). We demonstrate that by modulating the pore radius in between pore intersections, the PBG can be doubled in size to nearly 16%. The enlarged PBG is robust against a number of structural perturbations.

DOI: 10.1103/PhysRevE.68.046607 PACS number(s): 42.70.Qs

I. INTRODUCTION

Photonic band-gap (PBG) materials are crystals with periodic arrangements of the dielectric constant. This periodicity causes Bragg scattering, which along with microscopic scattering resonances forbids electromagnetic waves of a certain spectral region from propagating in the crystal [1,2]. This property makes PBG materials attractive for use in integrated optical circuitry. For example, it is possible through light localization to guide light in micron-scale, single-mode air-waveguide channels, without recourse to the more conventional mechanism of total internal reflection (refractive index guiding). By engineering of the local electromagnetic density of states, PBG materials also facilitate frequency selective control over spontaneous emission of light from atoms. As a result, active devices such as zero threshold lasers [3] and possibly all-optical transistors [4] may be integrated with the waveguide network on chip.

The challenge remains, however, to efficiently produce large wafer-scale structures with full, three-dimensional band gaps centered near 1.55 μm, the wavelength of choice in optical telecommunications. The lattice constant for the dielectric structure scales with the wavelength of the band gap, and hence crystals used in optical circuits must have submicron lattice constants. At the same time, the practical and commercial benefits of PBG materials necessitate efficient, low-cost manufacturing of very high quality, centimeter scale, semiconductor wafers.

Early considerations of photonic band structure focused on the face-centered-cubic (fcc) lattice [1,2,5]. It was pointed out [6], however, that the creation of a PBG between the lowest possible bands requires a breaking of spherical symmetry within the fcc unit (Wigner-Seitz) cell. This led to the fabrication [5] of a fcc lattice of crisscrossing pores drilled into Plexiglas and exhibiting a PBG in the microwave spectrum. This structure is conceptually straightforward to implement: a triangular lattice is defined on the [1,1,1] plane of the material, and three pores are grown from each lattice point, one each in the (0,1,1), (1,0,1), and (1,1,0) directions. While the fcc lattice was earlier fabricated in the microwave regime using conventional drill bits, it has proven difficult to produce pores with the submicron radii required for a PBG in the optical regime. Electron beam lithography and reactive ion etching methods [7,8] have been used to produce such pores, but only a few periods of the structure were produced, and there was severe degradation of the structure at the pore crossing points. On the other hand, experiments with x-ray lithography [9] have produced structures with lattice constants in the 10–50 μm range in polymer photoresists. These templates would require replication with a high refractive index semiconductor such as silicon. Even if this secondary replication step could be performed, the resulting PBG would occur in the 25–125 μm range.

The difficulties in synthesizing three-dimensional (3D) PBG materials with a gap near 1.5 μm have been addressed using several independent approaches. The first relies on layer-by-layer growth and stacking of two-dimensional (2D) photonic crystals in a ''woodpile'' architecture [10–13]. While wafer-scale structures have been made in silicon [11] using this approach, the method is tedious and it is difficult to grow the structure for a depth of more than three unit cells before the woodpile rods exhibit misalignment. Another approach relies on the self-assembly of silica spheres into a fcc opal lattice. This template is then ''inverted'' by chemical vapor deposition of silicon and selective etching of the opal template [14–16]. While this silicon ''inverse opal'' can be synthesized efficiently on a large scale, the resulting PBG is only about 5% of the gap center frequency in practice and is vulnerable to disorder effects. A third approach using glancing angle deposition techniques [17] leads to the formation of square spiral posts consisting of silicon on a silicon substrate. A PBG as large as 24% of the gap center frequency has been predicted [18,19] for suitably architectured square spiral posts. In this paper, we discuss a new PBG blueprint based on the remarkable discovery [20] that a stretched fcc lattice can be fabricated using photoelectrochemical etching in single-crystal Si. Photoelectrochemical etching yields pores with high length-to-diameter aspect ratios in the range 100–500 [21]. In the etching process [22,23], pore tips are formed on the etching surface, for instance, by photolithography and alkaline etching. The surface with the pore tips is exposed to a dissolving solution, often HF, while the opposite (back) face is illuminated. The light absorption from the

illumination generates electronic holes, which diffuse to the etching surface and are consumed at the pore tips. This promotes dissolution of the material at the pore tips, which in turn grows the pores. The pore radius is controlled only by the amount of illumination. Macropores formed using this technique grow in the (1,0,0) direction when the etching surface is normal to (1,0,0) and in the $\langle 1,1,3\rangle$ family of directions when the etching surface is the [1,1,1] crystallography surface. To generate the crisscrossing pore structures discussed here, three pores from the $\langle 1,1,3\rangle$ family are grown from points on a triangular lattice defined on the [1,1,1] plane of the material, resulting in a fcc lattice that is ''stretched'' in the [1,1,1] direction. We refer to this structure as ''Kielovite.'' Unfortunately, this deformation results in a crystal with a smaller PBG than that of the undistorted fcc lattice. However, this etching process allows for modulation of the pore radius along the growth direction. Increasing the illumination increases the overall charge carrier current from the back face to the etching face. Since the number of pore tips remains the same, the pore radius increases in response and thus can be accurately controlled by the amount of illumination. Structures incorporating such modulation have already been demonstrated in 2D photonic crystals [24]. In this paper, we demonstrate that a suitable pore modulation in the 3D distorted fcc (Kielovite) structure can yield a PBG of nearly 16% of the gap center frequency.

II. PHOTONIC BAND STRUCTURE OF KIELOVITE

We consider first the naturally occurring Kielovite structure, with no modulation of the pore radius. In this case the only structural parameter to adjust is the overall pore radius, which in turn determines the volume filling fraction of solid material. For simplicity we consider a material with a dielectric constant of 11.9, which corresponds to that of silicon. In contrast, the pores are taken to be filled with air. Band structures are calculated using the plane wave expansion method described in Ref. [6] with over 720 plane wave directions (over 1440 plane waves in total). The results are practically indistinguishable from those obtained for the same structures using over 1300 plane wave directions. The Fourier coefficients of the dielectric structure are calculated using a discrete Fourier transform with 256 points per direction.

The structure is modeled using a hexagonal lattice, which is defined by primitive lattice vectors $\vec{a}_1 = a(\frac{1}{2}, -\sqrt{3}/2, 0)$, $\vec{a}_2 = a(\frac{1}{2}, \sqrt{3}/2, 0)$, and $\vec{a}_3 = c(0,0,1)$. For our structure, we define the etching surface to be the xy plane, with a being the lattice constant of the triangular lattice. The length of $\vec{a}_3$ is prescribed by the angles between the etching surface normal and the pores. For Kielovite, $c/a = \frac{5}{2}\sqrt{3/2} = 3.06$. Figure 1 shows a schematic diagram of Kielovite, including a modulation in the pore radius, which is discussed later. The reciprocal lattice is likewise a hexagonal lattice and the Brillouin zone is shown in Fig. 2, with the high-symmetry points labeled. It is important to note that the fcc lattice of crisscrossing pores has an irreducible Brillouin zone (IBZ) which is the same as that of the fcc Bravais lattice. However, the same is not true for Kielovite. Due to the deformation in the direction perpendicular to the etching surface, the IBZ of Kielovite is considerably larger than the fcc Bravais lattice.

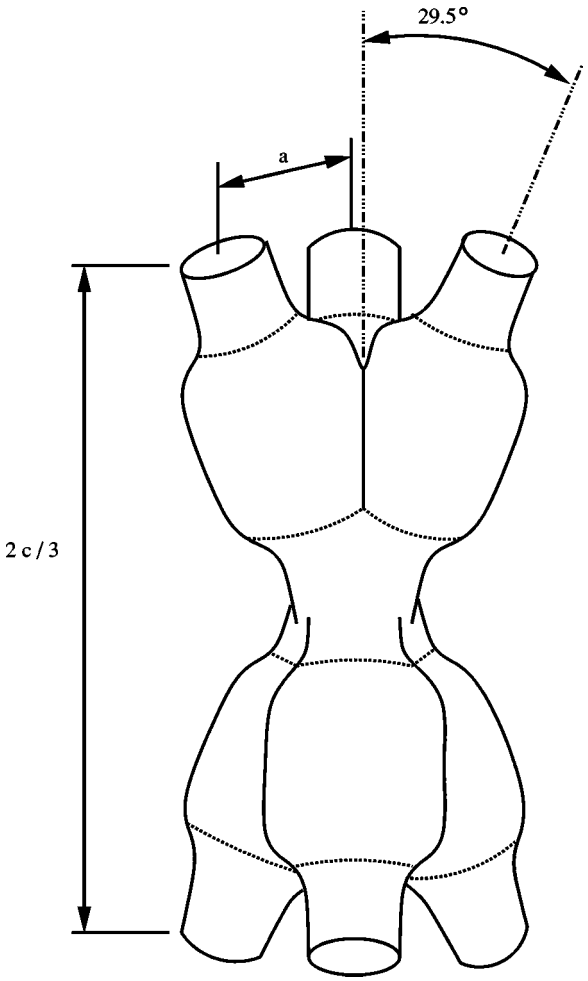

FIG. 1. Schematic diagram of Kielovite, showing the intersection between three pores. The angle between the pores and the vertical lattice vector is 29.5°. The lattice constant of the triangular etching mask is denoted by a and c denotes the lattice constant in the perpendicular direction.

Figure 3 shows the band structure of Kielovite with no pore radius modulation, at a volume filling fraction of 79% air, which optimizes the band gap. The pores have radius $0.34a$, where a is the lattice constant of the triangular lattice on the etching surface. The resulting PBG, denoted by the hashed area on the figure, is only 8%, roughly half the optimized PBG for the fcc lattice with the same dielectric contrast. The origin of the narrowing of the PBG is clearly seen to be the lowering of the fifth and sixth bands at the A point. Here, the difference in the IBZ between our structure and the fcc lattice of pores is important: if one considers only the IBZ of the fcc lattice, then this A point is irrelevant.

III. OPTIMIZATION OF THE PBG BY PORE MODULATION

In order to increase the PBG of the structure, we introduce a modulation in pore radius, symmetrically placed in between pore intersections. Figure 4 shows a schematic side

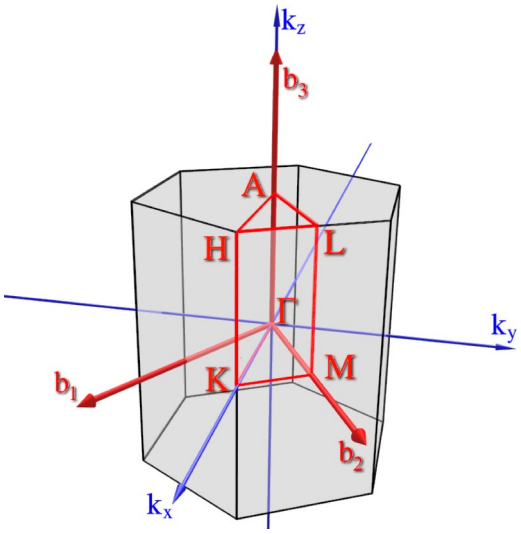

FIG. 2. First Brillouin zone of the Kielovite is shown as a shaded hexagonal prism, along with the primitive vectors $\vec{b}_1$, $\vec{b}_2$, and $\vec{b}_3$ of the reciprocal lattice. The section (triangular prism) denotes the irreducible Brillouin zone, which is 1/24 of the volume of the full zone. High-symmetry points are labeled as A, H, K, L, and M.

view of a pore with such a modulation, in the region between intersections with two other pores. The expanded pore radius occurs over a length w. The amplitude of the modulation is denoted as A, while the bare pore radius is denoted by r. We characterize a structure with a step modulation using these three parameters. The dotted curves show the structure with the same $[r,A,w]$ parameters but with a nonzero healing length h. For a given volume filling fraction, choosing any two of r, A, or w constrains the third. The modulation amplitude can be either positive (as pictured) or negative, the latter case implying a decrease in the pore radius over the width of the modulation.

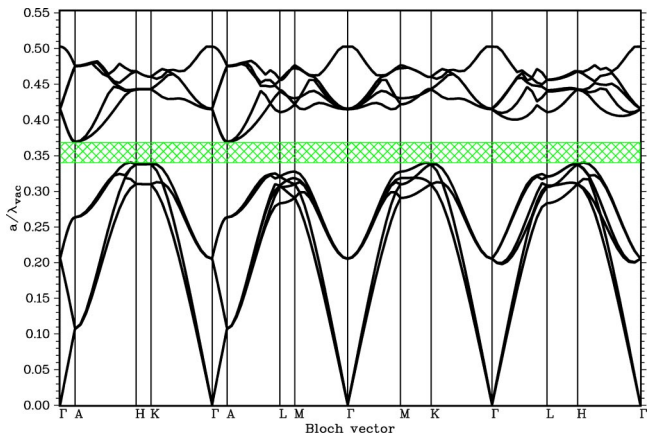

FIG. 3. Band structure for Kielovite in a background dielectric constant of 11.9 (silicon). Here the pore radius is $0.34a$, where "a" is the triangular lattice constant of the etching surface (separation between etch pits). The volume filling fraction is 79% air and the resulting PBG (hashed area) has a width of 8.0% of the center frequency.

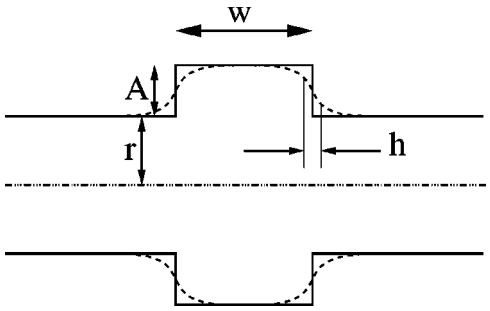

FIG. 4. Schematic side view of pore with radius modulation of longitudinal extent w and transverse amplitude A. The bare pore radius is r. The dashed curves represent the modulation with a healing length h. The ends represent the intersections with other pores.

Figure 5 shows the photonic band structure for a crystal with modulation of the pore radius, characterized by $[r,A,w]=[0.26,0.11,0.305]$, implying a volume filling fraction of 79% air. For a background dielectric constant of 11.9 (silicon), the width of the PBG is 15.5% relative to the center frequency. Clearly the droop in the fifth and sixth bands at the A point has diminished as a result of pore modulation. This is nearly as wide as the fcc lattice of crisscrossing pores with the same contrast in dielectric constants. Figure 5 is representative of the largest PBG we find in the given parameter space. In contrast, we find that structures with negative A have a smaller optimum PBG of 12% of the center frequency.

Figure 6 shows the dependence of the PBG on the background dielectric constant for the optimized structure characterized by $[r,A,w]=[0.26,0.11,0.305]$, as in Fig. 5. One can see that the PBG width initially increases dramatically as the dielectric contrast is increased, and then begins to saturate at large dielectric contrasts.

IV. ROBUSTNESS OF THE PBG TO STRUCTURAL PARAMETER MODIFICATIONS

We find there is a great deal of flexibility in choosing parameters in order to approach the upper bound for the PBG

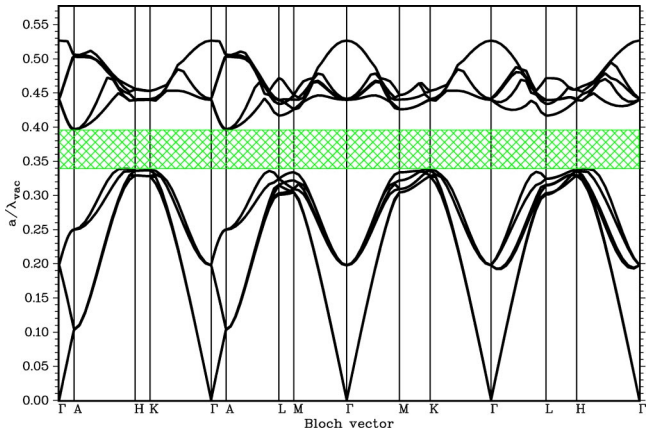

FIG. 5. Photonic band structure of Kielovite with positive pore radius modulation, characterized by $[r,A,w]=[0.26,0.11,0.305]$. The volume filling fraction is 79% air, and the resulting PBG is 15.5% relative to the center frequency for a background dielectric constant of 11.9 (silicon).

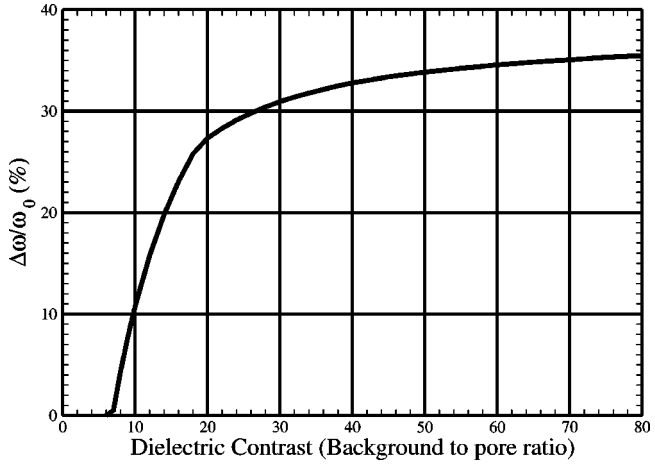

FIG. 6. Dependence of the PBG on the dielectric contrast for Kielovite with positive pore radius modulation characterized by $[r,A,w]=[0.26,0.11,0.305]$, where these lengths are given in units of the lattice constant a. The volume filling fraction is 79% air.

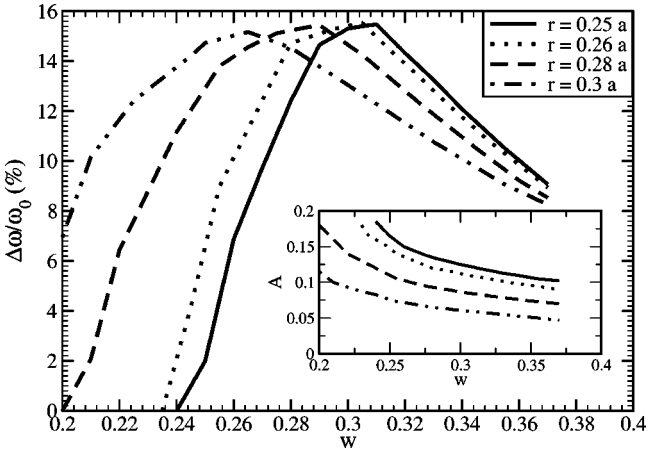

FIG. 8. Effect of varying the modulation width w on the band gap at various r, with corresponding A values shown in the inset. Volume filling fraction is fixed at 79% air. Lengths are given in units of the lattice constant a.

width. This, in turn, suggests considerable robustness of the optimized PBG to structural parameter variations and random disorder effects.

Figure 7 shows the effect of changing A on the PBG width at various r, with a fixed volume filling fraction of 82% air. The inset shows the values of w required for the given r, A and filling fractions. Clearly a large band gap can be achieved using several different configurations.

Figure 8, on the other hand, shows the effect of varying w at fixed r, with volume filling fraction 79% air and A constrained by these parameters. Again, the upper bound on the filling fraction is reached at several w.

Finally, the effects of varying r are shown in Fig. 9. In this case, the volume filling fraction is also changed, and we see that the upper bound is reached at a volume filling fraction of 79%.

It is important to note the effect of disorder in the structural parameters on the PBG. As a result of the fabrication process, small, random variations in the r, A, and w parameters are likely to appear along the periodic structure. The effect of this can be studied by considering the shift in the band edge frequencies as the structural parameters are varied. The resulting PBG in a structure with weak disorder in these parameters will then be given by the intersection of the PBGs of the perfectly ordered structures whose parameters span the distribution present in the disordered structure [25].

Figures 10 and 11 show the band edges as functions of the structural parameters in perfectly ordered structures, with initial geometries corresponding to $[r,A,w]=[0.26,0.11,0.305]$ and $[r,A,w]=[0.30,0.07,0.265]$, respectively. One can see that the band edges are most sensitive to changes in the bare pore radius r.

A particularly important issue is the robustness of the PBG to gradual variations (nonzero healing lengths in the step modulation) of the pore radius. Such a gradual change in pore radius is inevitable in the photoelectrochemical etching

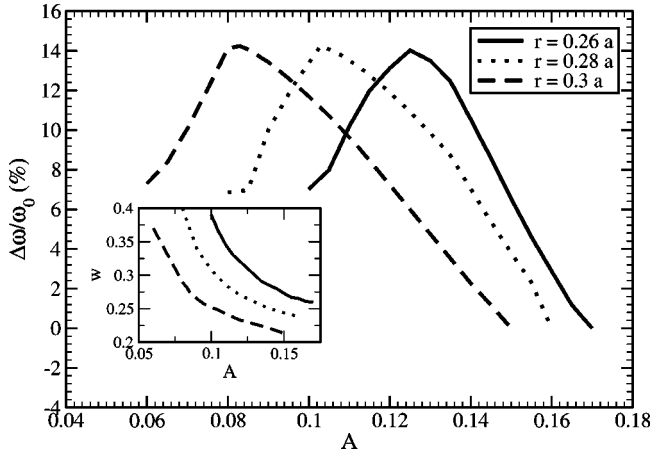

FIG. 7. Effect of the modulation amplitude A on the band gap at various r, with corresponding w values shown in the inset. Volume filling fraction is fixed at 82% air. Lengths are given in units of the lattice constant a.

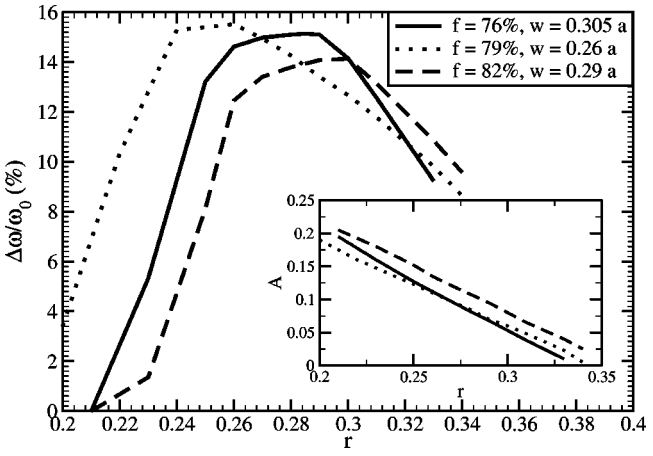

FIG. 9. Effect of varying the bare pore radius r on the band gap at various w and volume filling fractions, with corresponding A values shown in the inset. Lengths are given in units of the lattice constant a.

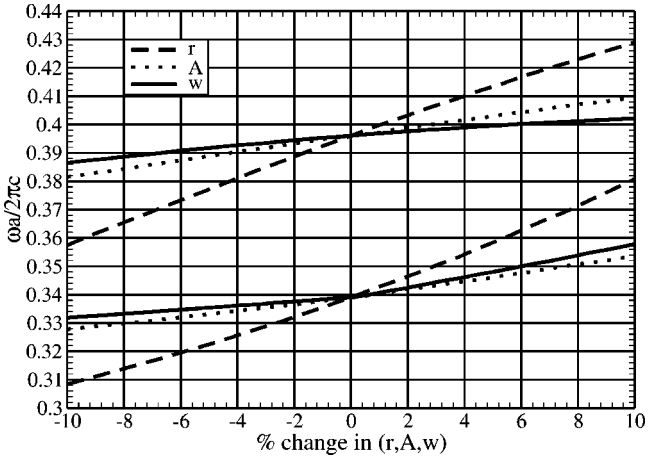

FIG. 10. The band edges as a function of change in the structural parameters, *r*, *A*, and *w*. The relative change is given as a percentage of the initial value. The initial geometry is characterized by $[r,A,w]=[0.26,0.11,0.305]$, with the lengths measured in units of the lattice constant *a*.

process. This is modeled by using the hyperbolic tangent function to represent steps.

Figure 12 shows the effects of the healing length on the PBG width for $[r,A,w]=[0.26,0.11,0.305]$ and $[r,A,w]=[0.30,0.07,0.265]$. In both cases, the relative PBG width remains above 15% until the healing length reaches about $0.1a$. Clearly, the PBG remains robust to realistic smoothing effects in the step modulation of the pore radius.

Besides the centered step increases and decreases between pore intersections, we have also explored other modulations to the pore radius, with varying degrees of success with respect to increasing the PBG. For single-step increases and decreases, a centralized modulation (symmetrically placed between adjacent pore crossings) produces a larger PBG than asymmetric modulations. Moving the modulation from the center point between pore intersections decreases the gap.

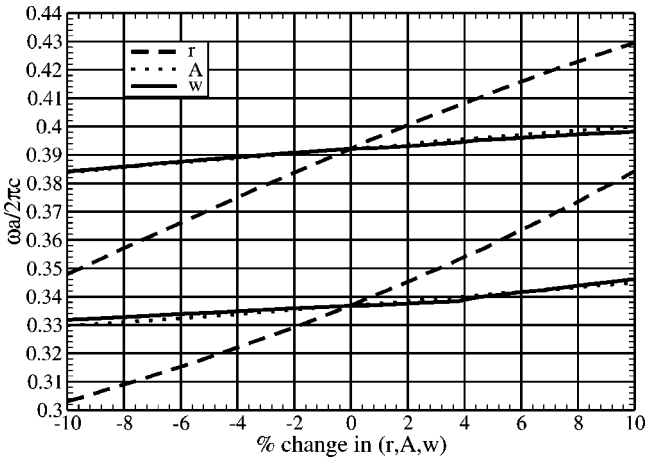

FIG. 11. The band edges as a function of change in the structural parameters *r*, *A*, and *w*. The relative change is given as a percentage of the initial value. The initial geometry is characterized by $[r,A,w]=[0.30,0.07,0.265]$, with the lengths measured in units of the lattice constant *a*.

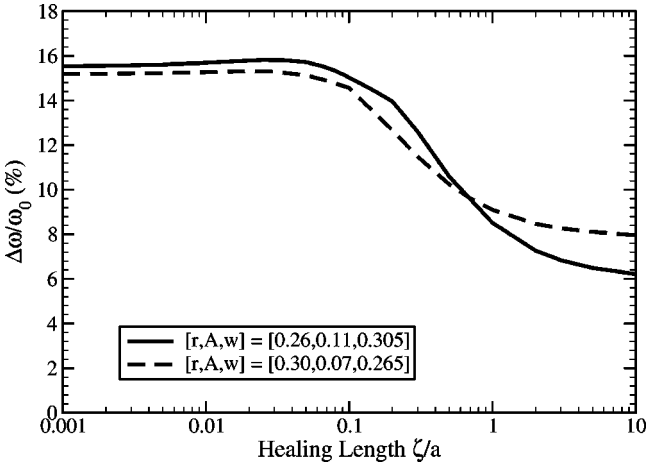

FIG. 12. Variation of the PBG width on the healing length of step modulations, at a nominal volume filling fraction of 79%.

Introducing a second-step modulation into the pore radius also does not increase the gap to the same level as the single, centered, step increase. For such situations, the gap increases as the parameters tend towards the case of the single-step increase. Finally, introducing a small sinusoidal modulation to the pore radius, along the entire length of each pore, increases the relative gap from the 8% to the 11% range. This falls short of the nearly 16% PBG resulting from the more localized step modulations we have described above.

V. DISCUSSION

Crisscrossing pore structures created by photoassisted electrochemical etching offer a unique opportunity for low cost, wafer-scale 3D PBG materials in a variety of group IV and III-V semiconductors. These materials consist of semiconductor single crystals and may be suitable for electrical pumping through the solid backbone and various optoelectronic applications. The photoelectrochemical etching method is unique, in that it allows pore depths of several hundred microns on large area wafers. For PBGs centered in the 800 nm$-$1.55 μm range, this corresponds to more than 10^4 unit cells of photonic crystal in each of the transverse directions and more than 100 unit cells in the vertical direction. Using realistic pore modulations, we have demonstrated that a complete 3D PBG spanning up to 16% of the center frequency is attainable in a number of important semiconductor materials, including Si, GaAs, and InP.

The use of optimized, Kielovite, PBG materials for optical microcircuitry requires the incorporation of planar, line, and point defects into the otherwise 3D periodic lattice. A planar (2D microchip) effect can be introduced by means of larger or smaller modulation of each of the pores at a specified depth into the wafer. Line defects (optical waveguide channels) and point defects (optical micro-cavities) may be introduced by means of focused ion beam exfoliation of the semiconductor backbone at specified locations.

It is also of considerable interest to microfabricate active regions within the 3D PBG wafer. This might be achieved by means of planar quantum dot layers (for instance, InAs dots

in InP) buried within the semiconductor wafer, prior to electrochemical etching. Photonic band-gap properties may also be tuned through ultrafast processes such as free-carrier injection through optical pulses at frequencies above the PBG and above the electronic semiconductor gap of the PBG backbone [26].

These considerations suggest a broad spectrum of opportunities for Kielovite PBG materials. The realization of a 16% complete 3D PBG on wafer-scale samples using the prescribed pore modulation during the photoelectrochemical etch would be a major advance relative to the more widely studied 2D macroporous silicon photonic crystals [21]. The realization of this 3D PBG in a *single-crystal* semiconductor of more than 100 μm depth would also be a unique achievement in the field of photonic crystals.

ACKNOWLEDGMENTS

We are grateful to Ovidiu Toader, Helmut Föll, Volker Lehmann, Ralf Wehrspohn, Ulrich Gösele, and Jörg Schilling for a number of stimulating discussions. This work was supported in part by the National Sciences and Engineering Research Council (NSERC) of Canada. T.Y.M.C. acknowledges financial support from NSERC. S.J. acknowledges the hospitality of the Max Planck Institute for Microstructure Physics in Halle, Germany.

[1] Sajeev John, Phys. Rev. Lett. **58**, 2486 (1987).
[2] Eli Yablonovitch, Phys. Rev. Lett. **58**, 2059 (1987).
[3] Jonathan P. Dowling, Michael Scalora, Mark J. Bloemer, and Charles M. Bowden, J. Appl. Phys. **75**, 1896 (1994).
[4] Sajeev John and Marian Florescu, J. Opt. A: Pure Appl. Opt. **3**, S103 (2001).
[5] E. Yablonovitch, T.J. Gmitter, and K.M. Leung, Phys. Rev. Lett. **67**, 2295 (1991).
[6] K.M. Ho, C.T. Chan, and C.M. Soukoulis, Phys. Rev. Lett. **65**, 3152 (1990).
[7] C.C. Cheng and A. Scherer, J. Vac. Sci. Technol. B **13**, 2696 (1995).
[8] C.C. Cheng, A. Scherer, V. Arbet-Engels, and E. Yablonovitch, J. Vac. Sci. Technol. B **14**, 4110 (1996).
[9] G. Feiertag *et al.*, Appl. Phys. Lett. **71**, 1441 (1997).
[10] E. Özbay, A. Abeyta, G. Tuttle, M. Tringides, R. Biswas, C.T. Chan, C.M. Soukoulis, and K.M. Ho, Phys. Rev. B **50**, 1945 (1994).
[11] S.Y. Lin *et al.*, Nature (London) **394**, 251 (1998).
[12] S. Noda, K. Tomoda, N. Yamamoto, and A. Chutinan, Science **289**, 604 (2000).
[13] C.T. Chan, K.M. Ho, C.M. Soukoulis, R. Biswas, and M. Sigalas, Solid State Commun. **89**, 413 (1994).
[14] H. Míguez, A. Blanco, F. Meseguer, C. López, H.M. Yates, M.E. Pemble, V. Fornés, and A. Mifsud, Phys. Rev. B **59**, 1563 (1999).
[15] A. Blanco *et al.*, Nature (London) **405**, 437 (2000).
[16] Yu.A. Vlasov, V.N. Astratov, A.V. Baryshev, A.A. Kaplyanskii, O.Z. Karimov, and M.F. Limonov, Phys. Rev. E **61**, 5784 (2000).
[17] Scott R. Kennedy, Michael J. Brett, Ovidiu Toader, and Sajeev John, Nano Lett. **2**, 59 (2002).
[18] Ovidiu Toader and Sajeev John, Science **292**, 1133 (2001).
[19] Ovidiu Toader and Sajeev John, Phys. Rev. E **66**, 016610 (2002).
[20] M. Christophersen, J. Carstensen, A. Feuerhake, and H. Föll, Mater. Sci. Eng., B **B69**, 194 (2000).
[21] J. Schilling *et al.*, J. Opt. A: Pure Appl. Opt. **3**, S121 (2001).
[22] U. Grüning, V. Lehmann, and C.M. Engelhardt, Appl. Phys. Lett. **66**, 3254 (1995).
[23] S. Rowson, A. Chelnokov, C. Cuisin, and J.-M. Lourtioz, IEE Proc.: Optoelectron. **145**, 403 (1998).
[24] J. Schilling, F. Müller, S. Matthias, R.B. Wehrspohn, and U. Gösele, Appl. Phys. Lett. **78**, 1180 (2001).
[25] J. M. Ziman, *Models of Disorder* (Cambridge University Press, Cambridge, 1979), p. 345.
[26] S.W. Leonard, J.P. Mondia, H.M. van Driel, O. Toader, S. John, K. Busch, A. Birner, U. Gosele, and V. Lehmann, Phys. Rev. B **61**, R2389 (2000).